

Research Article

# Measurements Inside a Rabbit Sized FFL-MPI Device Using a Gradiometric Receive Coil

Jan Stelzner\* · Matthias Graeser · Anna Bakenecker · Anselm von Gladiss · Gael Bringout · Thorsten M. Buzug

Institute of Medical Engineering, Universität zu Lübeck, Lübeck, Germany

\*Corresponding author, email: stelzner@imt.uni-luebeck.de

Received 25 November 2016; Accepted 25 February 2017; Published online 23 March 2017

© 2017 Stelzner; licensee Infinite Science Publishing GmbH

This is an Open Access article distributed under the terms of the Creative Commons Attribution License (<http://creativecommons.org/licenses/by/4.0>), which permits unrestricted use, distribution, and reproduction in any medium, provided the original work is properly cited.

## Abstract

This work continues prior investigations on the currently world's largest field-free line (FFL) magnetic-particle-imaging (MPI) scanner. The bore of the imaging device provides a diameter of 180 mm and is designed to accommodate measurement objects up to rabbit size. It has already been shown that the drive-field coil is capable of conducting an alternating current with a frequency of 25 kHz and an amplitude of above 500 A. With this current input, the drive-field generator produces a magnetic flux density of more than 20 mT amplitude in the center of the bore. As the associated magnetic field strength is already sufficient to excite super-paramagnetic iron oxide nano particles (SPIONs), this work presents an approach to further increase the sensitivity of the system by testing a gradiometric receive-coil arrangement.

## 1. Introduction

In 2008, a new concept of spatial encoding in Magnetic Particle Imaging (MPI) was presented by Weizenecker et al. [1]. It has been proposed to use a selection field that acquires the particle signal along a FFL instead of using a field-free point (FFP). However, as a scanner based on this original concept consumes too much electric power to be feasible, Knopp et al. presented a coil topology that was able to reduce the power consumption to a factor of 3.3 times the required power for an FFP scanner of equal size and gradient performance [2]. In 2012, Goodwill et al. provided first image reconstructions of different phantoms using projections that were taken by a permanent-magnet FFL [3]. In 2014, Bente, Weber et al. set up a device featuring an electronically rotating FFL and proved the feasibility of this advanced concept to show imaging

results providing high spatial and temporal resolution [4]. One year later, Bringout et al. presented a concept of a rabbit-sized FFL-scanner (see Fig. 1) [5]. This field generator with its 180 mm bore diameter is designed to generate an electronically rotating FFL with a gradient strength of 0.8 T/m and a drive-field amplitude of 15 mT.

Recent results have already shown measurements of the amplitude spectrum produced by the rabbit-sized FFL-MPI scanner [6]. These measurements were performed without using a dedicated receive coil, meaning that the drive-field generator simultaneously functioned as a receive coil. Until this work, the prospects of employing a dedicated coil to pick up the particle signal within this particular setup was not taken into account. One advantage can be achieved, when the receive coil is designed as a magnetic gradiometer. The usability of gradiometric receive coils has been shown in [7].

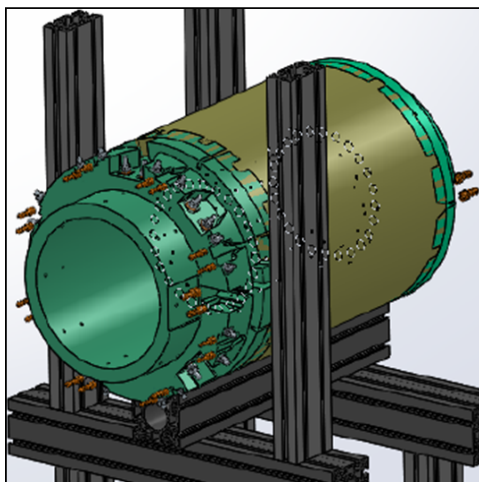


**Figure 1:** CAD model of the rabbit sized FFL-MPI scanner.

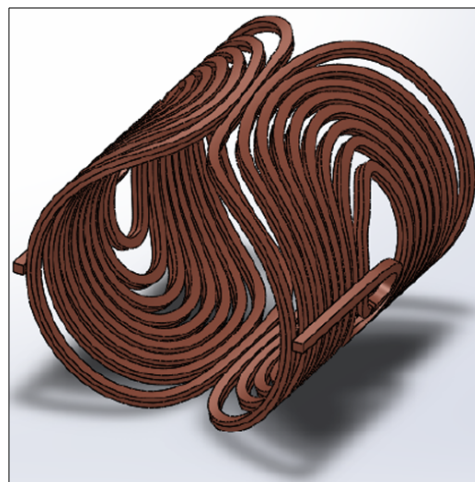


**Figure 2:** CAD model of the drive-field coil.

In this work, current investigations on this imaging device are presented. In the second section, two different measurement setups are described, that characterize the magnetic field that is produced by the drive-field generator and its effect on a gradiometric receive coil arrangement. In the third section of this work, the measurement results are presented and annotated. Please note that all measurements were taken in the absence of a selection field.

## II. Materials and Methods

### II.I. Drive-Field Measurement

The drive-field coil assembly consists of two pairs of saddle coils, both in Helmholtz configuration, generating magnetic fields perpendicular to the bore axis. To achieve lower losses than in a homogeneous conductor, the drive-field coils, which are designated to conduct alternating currents of 25 kHz, are made of high-frequency litz-wire containing 10000 strands with a diameter of 63  $\mu\text{m}$ . One of the Helmholtz configurations is dedicated to the translation of the FFL in horizontal direction as the other pair effects the vertical translation. The drive-field generator was assembled and designed in the Institute of Medical Engineering at the University of Luebeck based on the approach of Bringout et al. [8]. The wire path of a drive-field coil-pair for the horizontal direction is illustrated in Fig. 2.

A crucial criterium for a well suited drive-field generator in MPI is a high homogeneity of the magnetic flux density provided within the field of view. Therefore, the magnetic field was measured beforehand feeding the field generator by a direct current of 50 A and using a 3D hall probe to acquire the vector components of the magnetic flux. To measure at different positions, the hall probe was mounted on a robot arm (see Fig. 3).

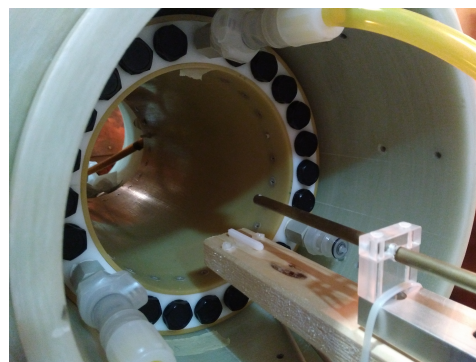


**Figure 3:** Measurement of the magnetic field of the drive-field generator. The magnetic flux density at different positions is measured by the hall probe that is mounted on a robot.

### II.II. Receive Coil Configuration

The basic idea behind the enhancement of the signal quality of the described system is the use of a cylindrical second order gradiometer. The functional principle of an electromagnetic gradiometer is rather simple. In this approach, the configuration consists of a cylindrical receive coil in the center and two concentric compensation coils with opposite winding direction, one that is above and a similar one below the center receive coil, respectively (see Fig. 4).

Assuming a homogeneous magnetic field like the drive field for instance, the induced voltage in the center coil is superimposed by the compensation coils' voltages so that the entire induced voltage by the drive field follows the equation

$$V_{\text{DF}} = \frac{\partial}{\partial t} \cdot (\psi_{\text{Rx}} + \psi_{\text{C1}} + \psi_{\text{C2}}) = 0 \quad (1)$$

with  $\psi_{\text{Rx}}$  being the induction flow through the center receive coil and  $\psi_{\text{C1}}$  and  $\psi_{\text{C2}}$  the induction flow through the compensation coils. Due to the different winding



**Figure 4:** Second order magnetic gradiometer with a center coil and two compensation coils on the left hand and right hand side.

directions and proper dimensioning, the superimposed voltage becomes zero. Considering a particle sample inside this assembly, the desired signal harmonics that the particles introduce can still be seen owing to the field inhomogeneity they cause.

The induced signal of the real drive field on the gradiometer is investigated and measured at different positions. To find the ideal position of the gradiometric receive coil assembly, an additional reference coil is used that is similar to the center coil of the gradiometer and is just wound above it to measure the amount of the magnetic flux density along the axial direction of the receive coil configuration (see Fig. 5). The rotational axis of the receive-coil assembly is at each measurement perpendicular to the bore axis and collinear to the ideal magnetic field direction of the operating drive-field coil-pair. Further adjustments can be attained by adding or removing single windings from the compensation coils or rotating the drive-field generator inside the surrounding selection-field generator housing.

The drive-field generator of the rabbit-sized scanner is fed by a function generator, that provides a sinusoidal signal of  $f_E = 25$  kHz. It is matched by a serial capacitor  $C_S$  and a parallel one  $C_P$  which transform the impedance of the drive field generator to an ohmic load of  $R_S = 2 \Omega$  at the excitation frequency. Additionally, they offer an exceptionally narrow bandwidth making the network act like a frequency filter as the voltage transfer of the third harmonic is about 25 dB lower than the voltage transfer of the fundamental. This enables the drive field coil to provide a fairly clean sinusoidal field generation, even with a distorting signal source. The dimensioning of the capacities follows the equations

$$C_S = \left( \omega_E^2 L_{DFC} - \omega_E \cdot \sqrt{R_{DFC}(R_S - R_{DFC})} \right)^{-1} \quad (2)$$

and

$$C_P = \left( \omega_E \cdot \sqrt{\frac{R_{DFC}}{R_S - R_{DFC}} R_S} \right)^{-1}, \quad (3)$$

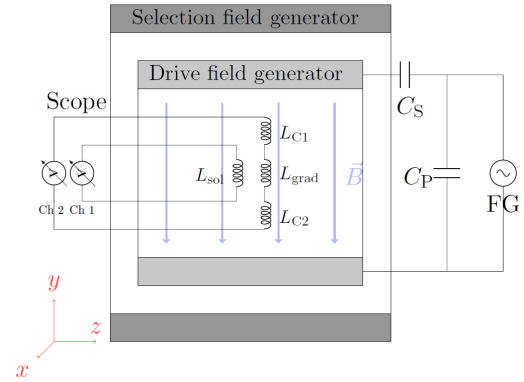


**Figure 5:** Schematic illustration of the gradiometer measurement-setup. The scanner bore is aligned to the  $z$  axis. The gradiometer itself is represented by 3 serial inductors  $L_{C1}$ ,  $L_{grad}$ , and  $L_{C2}$ . An additional inductor  $L_{sol}$  is used as a solenoidal reference coil. The orientation of the vertical drive field  $\vec{B}$  is aligned to the  $y$ -axis just as all inductors of the receive-coil assembly. The drive-field generator, which is surrounded by the selection-field generator of the FFL scanner, is matched by the capacitors  $C_S$  and  $C_P$  to the function generator (FG). The induced signals are measured and displayed simultaneously.

where  $L_{DFC}$  is the inductance of the drive-field coil,  $R_{DFC}$  is its equivalent serial resistance and  $\omega_E = 2\pi f_E$  the angular frequency of the excitation frequency. Please note, that Eq. (3) and Eq. (2) are only reasonable if  $R_S > R_{DFC}$ .

As the location of the receive coil-assembly is varied by the robot, the induced signals can be read out from an oscilloscope (see Fig. 6) to obtain an insight of the magnetic flux distribution or acquire measurements that represent the field profiles along each coordinate axis, respectively.

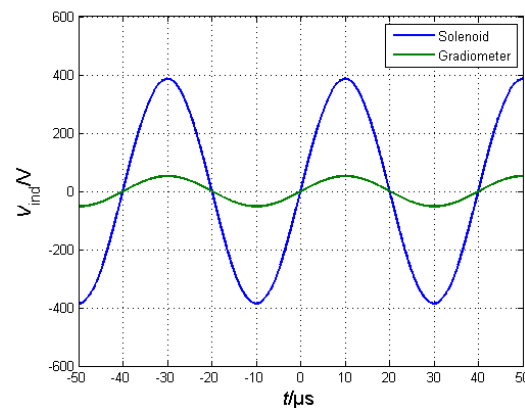


**Figure 6:** Recorded signals from the receive coil-assembly for one single position within the bore. The blue line is the induced voltage over the reference coil and has an amplitude of 386 mV<sub>p</sub>, the green one is the voltage over the gradiometer with 52 mV<sub>p</sub>.

### III. Results

#### III.I. Drive-Field Generator

The measurements of the static representation of the vertically oriented drive field is depicted in Fig. 7.

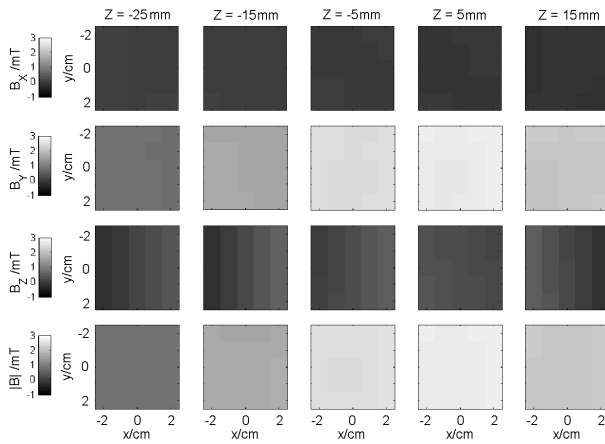


**Figure 7:** Magnetic field generated by the vertically oriented drive-field coil at different positions measured by the hall probe. The measurement grid consists of  $5 \times 5 \times 5$  voxels and  $4 \times 4 \times 40$  cm<sup>3</sup>, respectively. The nomenclature of the axes is similar to the one in Fig. 5. Each of the first three rows depicts a vector component of the magnetic flux density and the bottom row its amount. Each column represents a different location along the axial direction. The location (0/0/0) marks the center of the bore.

As anticipated, the amount of the magnetic flux density of the drive field exhibits a good homogeneity. The variation coefficient

$$c_V = \frac{\sigma}{\mu} \quad (4)$$

of the obtained values of  $|B|$  for a single slice of the measurement is below 1.06 % for  $|Z| = 5$  mm and for  $Z = -25$  mm still below 2 %.  $\sigma$  describes the standard deviation of the measured values within one slice and  $\mu$  their mean value. The vectorial quantity of the magnetic field is predominantly determined by its  $y$ -component inside the measurement region. The mean value of the ratio between  $B_y$  and  $|B|$  amounts to 98.85 %. In the same way the horizontally oriented drive-field coil provides a homogeneous magnetic field strength in  $x$ -direction.

According to the measurement, in the center of the drive-field coil and its vicinity, the magnetic flux density amounts to about 2.7 mT, when the coil is fed with 50 A.

#### III.II. Measurements of the Receive-Coil Assembly

Supplying the drive-field coil for the vertical translation of the FFL, representations of the field profile along the  $x$ -,  $y$ -, and  $z$ -axis were recorded.

For that, the receive-coil assembly, containing the gradiometer as well as the solenoidal reference coil, were moved by a robot through the bore. The resulting induced voltages are illustrated in Fig. 8.

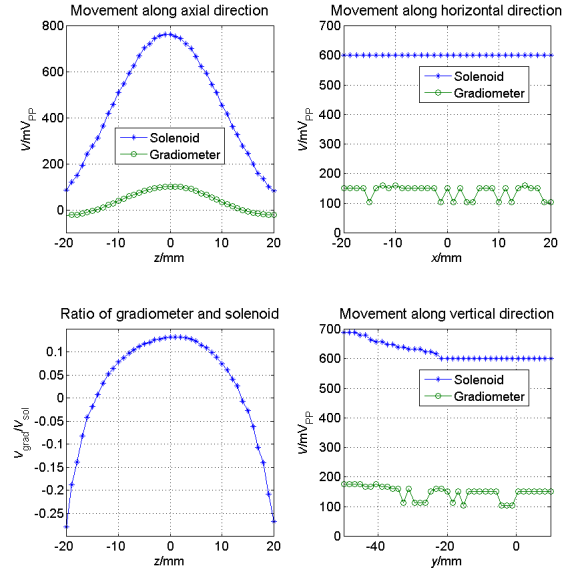


**Figure 8:** Induced voltage into the solenoidal and the gradiometric receive coil for various locations inside the field generator. The receive-coil assembly is aligned to the drive field pointing into  $y$ -direction. As one coordinate is varied at a time the other two coordinates are 0. The location (0/0/0) marks the center of the drive-field generator and the field of view, respectively.

As already shown in the previous section (see Fig. 7), the field and therewith the induced voltage along the radial directions is very homogeneous. Moving near the edge of the bore, a slight increase of the induced voltage can be observed. Translating the receive coils along the axial direction, a symmetrical behaviour to the center of the bore can be seen. The field of view in future imaging studies will be located in the center plane of the bore at  $z = 0$ . The ratio of the voltages over the gradiometer and the solenoid amounts to about  $1/8 = -18$  dB in the center of the bore and will be improved by a more appropriate design and adjustment of the compensation coils. A more accurate balancing of the gradiometer will reduce the overall induced voltage, which should be very close to 0 in the ideal case.

### IV. Conclusion

The use of a gradiometric coil assembly within the mentioned scanner setup is a promising method to increase its sensitivity as most of the disturbance is approximately homogeneous within the field of view. Further investigations, that will unveil whether this concept is actually

able to solve a cluster of problems appearing as higher harmonics in the absence of specimens will follow as no other approach so far like the enhancement of filtering circuits could work around adequately.

#### IV.I. Outlook

An electromagnetic gradiometer which is dedicated to the described MPI-FFL system will be constructed. It will be designed as an assembly of saddle coils similar to the drive field generator to fit the requirements of the scanner, provide a direct access to the field of view, and lead to better attenuation of the drive field in the absence of particle samples. Then, spectra of different particle samples can be obtained to prove and quantify the sensitivity gain of this concept. Finally, the receive-coil assembly will be extended to acquire two dimensional data.

#### References

- [1] J. Weizenecker, B. Gleich, and J. Borgert. Magnetic particle imaging using a field free line. *J. Phys. D: Appl. Phys.*, 41(10):105009, 2008. doi:[10.1088/0022-3727/41/10/105009](https://doi.org/10.1088/0022-3727/41/10/105009).
- [2] T. Knopp, T. F. Sattel, S. Biederer, and T. M. Buzug. Field-free line formation in a magnetic field. *J. Phys. A*, 43(1):012002, 2010. doi:[10.1088/1751-8113/43/1/012002](https://doi.org/10.1088/1751-8113/43/1/012002).
- [3] P. W. Goodwill, J. J. Konkle, B. Zheng, E. U. Saritas, and S. M. Conolly. Projection X-Space Magnetic Particle Imaging. *IEEE Trans. Med. Imag.*, 31(5):1076–1085, 2012. doi:[10.1109/TMI.2012.2185247](https://doi.org/10.1109/TMI.2012.2185247).
- [4] K. Bente, M. Weber, M. Graeser, T. F. Sattel, M. Erbe, and T. M. Buzug. Electronic field free line rotation and relaxation deconvolution in magnetic particle imaging. *IEEE Trans. Med. Imag.*, 34(2):644–651, 2015. doi:[10.1109/TMI.2014.2364891](https://doi.org/10.1109/TMI.2014.2364891).
- [5] G. Bringout, J. Stelzner, M. Ahlborg, A. Behrends, K. Bente, C. Debbeler, A. von Gladiss, K. Graefe, M. Graeser, C. Kaethner, S. Kaufmann, K. Lütke-Buzug, H. Medimagh, W. Tenner, M. Weber, and T. M. Buzug. Concept of a rabbit-sized FFL-scanner. In *International Workshop on Magnetic Particle Imaging*, 2015. doi:[10.1109/IWMP.2015.7107032](https://doi.org/10.1109/IWMP.2015.7107032).
- [6] J. Stelzner, G. Bringout, A. von Gladiss, H. Medimagh, M. Ahlborg, T. F. Sattel, and T. M. Buzug. First Spectrum Measurements with a Rabbit-Sized FFL-Scanner. In *International Workshop on Magnetic Particle Imaging*, 2016.
- [7] K. Murase, S. Hiratsuka, R. Song, and Y. Takeuchi. Development of a system for magnetic particle imaging using neodymium magnets and gradiometer. *Jpn. J. Appl. Phys.*, 53(6):067001, 2014. doi:[10.7567/JJAP.53.067001](https://doi.org/10.7567/JJAP.53.067001).
- [8] G. Bringout and T. M. Buzug. Coil Design for Magnetic Particle Imaging: Application for a Preclinical Scanner. *IEEE Trans. Magn.*, 51(2):5100808, 2014. doi:[10.1109/TMAG.2014.2344917](https://doi.org/10.1109/TMAG.2014.2344917).